Reaction Chemistry & Engineering

Design, Modelling, and Application of a Low Void-Volume in Situ Diffuse Reflectance Spectroscopic Reaction Cell for Transient Catalytic Studies

Journal:	*Reaction Chemistry & Engineering*
Manuscript ID	RE-ART-11-2018-000302.R1
Article Type:	Paper
Date Submitted by the Author:	14-Dec-2018
Complete List of Authors:	Patil, Bhagyesha; The University of Kansas, Department of Chemical & Petroleum Engineering; The University of Kansas, Center for Environmentally Beneficial Catalysis Srinivasan, Priya; The University of Kansas, Chemical & Petroleum Engineering Department; The University of Kansas, Center for Environmentally Beneficial Catalysis Atchison, Ed; The University of Kansas, Center of Environmentally Beneficial Catalysis Zhu, Hongda; The University of Kansas, Center of Environmentally Beneficial Catalysis Bravo-Suárez, Juan; The University of Kansas, Chemical & Petroleum Engineering Department; The University of Kansas, Center for Environmentally Beneficial Catalysis

Journal Name

ARTICLE

Design, Modelling, and Application of a Low Void-Volume in Situ Diffuse Reflectance Spectroscopic Reaction Cell for Transient Catalytic Studies

Via a Received 00th January 20xx,
Accepted 00th January 20xx

DOI: 10.1039/x0xx00000x

www.rsc.org/

Bhagyesha S. Patil,[a,b] Priya D. Srinivasan,[a,b] Ed Atchison,[b] Hongda Zhu,[b] Juan J. Bravo-Suárez*[a,b]

This paper describes a new low void-volume in situ reaction cell for use in diffuse reflectance spectroscopic studies. It was demonstrated by means of a residence time distribution analysis that the cell's average gas residence time was relatively small (~1.3 s) and within the time scale of rapid scan spectra sampling. Such combination enabled the rigorous implementation of transient periodic techniques such as modulation excitation-phase sensitive detection-diffuse reflectance Fourier infrared spectroscopy (ME-PSD-DRIFTS), which allowed unique access to surface reaction intermediates in gas-solid reactions. Application of the new cell and ME-PSD-DRIFTS to the conversion of ethanol on γ-Al_2O_3 at 200 °C demonstrated the presence of likely surface intermediate species that conform with ethanol conversion to diethyl ether via a SN2 mechanism and the involvement of several alumina hydroxyl types as possible active sites.

1. Introduction

In heterogeneous catalysis the in situ and operando characterization of catalysts at reaction conditions is a fundamental aspect required to understand elementary steps and the nature of active sites in catalyzed reaction mechanisms.[1-4] To accomplish such level of surface species understanding, the in situ characterization needs to use proper tools such as spectroscopic, microscopic, and diffraction techniques, laboratory reactors or reaction cells, and steady-state or transient methods such as steady-state isotopic transient kinetic analysis (SSITKA),[5-7] time-resolved spectroscopic techniques,[8-11] modulation excitation (ME) spectroscopy,[12-14] and/or their combinations.[12, 15] The most commonly utilized in situ and operando characterization techniques to identify catalyst active sites and reactive surface species include UV-visible, Fourier transform infrared, Raman, and X-ray absorption spectroscopies.[16-20] They are the workhorses among the arsenal of characterization tools available to catalysis researchers to support mechanistic proposals from kinetic and computational studies of heterogeneous catalytic reactions.[18] These spectroscopic techniques are most often applied to catalysts at reaction conditions in in situ or operando reaction cells,[21] although some techniques have also been applied directly to laboratory reactors.[16, 21]

While spectroscopic characterization of catalysts is desirable directly in laboratory reactors (because of well-established kinetically relevant measurements with them), this is often not possible due to mismatches between reactors and spectrometers geometry, differences between reactor and spectroscopic techniques catalyst particle size requirements, complex reactor modifications, and lack of long-life high temperature and pressure probes, among others.[1-3, 21-23] As a result, the main focus in the characterization of solid catalysts at reaction conditions has been by means of commercial or custom-made in situ and operando reaction cells that resemble laboratory reactors and which closely match the spectroscopic technique's space, time scale, or sample requirements.[2, 21-25] As in situ characterization techniques evolve from a tool to identify surface species (spectroscopic approach) to one that determines true kinetically relevant surface intermediates (spectrokinetic approach), reaction cell characteristics and performance need to match those expected in laboratory scale reactors in order to obtain meaningful catalytic information.[2, 3, 21, 23] This spectrokinetic approach, therefore, requires the demonstration that in situ cells operate in a manner similar to that of laboratory reactors. This can be accomplished by direct comparison of the kinetic analysis of a reaction in an in situ cell with that of a laboratory reactor, for example, at conditions that resemble operation in differential mode and in absence of mass and heat transfer artifacts.[2, 3, 21, 23] Once a reaction cell is demonstrated to operate under a strictly kinetic regime, identification of reactive surface intermediates can be carried out via in situ/operando spectroscopy combined with: 1) SSITKA (e.g., with FTIR),[6, 7] that operates at pseudo-steady state chemical potential;[6] 2) with ME that operates in continuous transient mode around a steady state;[12, 13] or 3) with pure transient methods where catalyst surface is tracked as surface

[a] Department of Chemical & Petroleum Engineering, The University of Kansas, Lawrence, KS, 66045, USA.
[b] Center for Environmentally Beneficial Catalysis, The University of Kansas, 1501 Wakarusa Dr., LSRL C145F, Lawrence, KS, 66047, USA. E-mail: jjbravo@ku.edu
†Electronic Supplementary Information (ESI) available. See
DOI: 10.1039/x0xx00000x

species coverage is changed from low or high coverage to steady state coverage or vice versa.[8-10]

Surface species that evolve during surface coverage or isotopic transients have been usually proposed as possible reaction intermediates; whereas those species that turn over at reaction rates similar to those in rate controlling steps are considered true surface reaction intermediates.[6, 8-11, 26-29] Identification of reactive species during in situ and operando experiments is not an easy task as it requires calibration of spectroscopic signals, which may not be trivial.[6, 9-11, 30] Even when performing typical difference spectra analysis between two different states (e.g., clean surface and covered surface at any time during a transient experiment), signals of surface intermediate species can be obscured by low signal-to-noise response or overwhelmed by the presence of abundant slow reactive or spectator species.[13, 31] A more modern approach has been the utilization of ME coupled with phase sensitive detection analysis during in situ spectroscopic characterization, which results in signals with enhanced signal-to-noise ratio while avoiding the presence of slow reacting or spectator species.[12-14, 31] ME and frequency response techniques have been also applied in the past to the characterization of catalysts and study of catalytic reactions.[32, 33]

In the concentration modulation excitation (cME) spectroscopy case, the method is characterized by rapid periodic changes (i.e., 1 period within about 100 s) in the feed concentration and rapid spectroscopic sampling (e.g., every 1 s) of surface species, which after PSD via Fourier transform analysis and filtering of signals that respond at the same frequency of the feed modulation, yields spectra with exclusively surface reactive species.[14, 34] To enable the cME-PSD methodology for fast transients such as those required in SSITKA and ME spectroscopy, the average residence time of gaseous species in spectroscopic reaction cells should be relatively fast (usually <1-2 s) and at space velocities similar to those found in lab scale reactors to ensure cell matching time scales for rigorous kinetic analyses while the spectroscopic sampling time should be within the same time scale. This is usually not an issue for gas-solid reactions in transmission cells which exhibit small dead volumes (<1 cm^3)[35, 36] and, thus, rapid gas feed exchanges at moderate feed flow rates of tens of cm^3/min.[21] While transmission spectroscopic reaction cells have been demonstrated to be adequate for operando and kinetic studies,[37] the small amount and pelletization of the catalyst sample, inhomogeneities in temperature and flow dynamics, and lack of resemblance to conventional fixed bed reactors are often a concern. Therefore, for application of cME-PSD methodology to catalyzed gas-solid reactions, diffuse reflectance (DR) based reaction cells are preferable.[21] However, the majority of current commercial DR reaction cells lack void volume characteristics similar to transmission cells. From a residence time distribution study, we showed recently that a modified commercial DR Harrick cell, with a reduced volume of ~3.5 cm^3 and total gas flow rates of 120 cm^3/min, exhibits gas mean residence times of ~4 s (different from the nominal space time $\tau_n = V/v \sim 1.8$ s).[38] This implies that lower gas mean residence times are achievable at gas feed flow rates well beyond 200 cm^3/min, which is quite high and could lead to backpressure in the cell and cell temperature inhomogeneities due to convective heat losses.[38, 39] Therefore, a low void-volume in situ DR reaction cell that can operate at moderate gas flow rates is highly desirable.

A few groups have reported ME-DRIFTS of gas-solid reactions in time resolved (TR) via difference spectra or PSD mode using homemade or modified commercial cells. These studies include early ME-TR-DRIFTS works by Wokaun and co-workers[40] (Spectra-Tech's[41] and Specac's[42, 43] reaction cells) and Davison and coworkers[44, 45] (homemade cell resembling that by Pike Technologies, except that gas flow did not go through the catalyst sample). More recent ME-PSD-DRIFTS works include those by Ferri and coworkers (Harrick's cell equipped with flat window,[46-48] homemade compact plug flow type cell with flat windows,[49] Specac's[50] and a modified Spectra Tech's reaction cell[51]), Baiker and co-workers[15, 31, 52] (homemade, low dead volume cell with flat windows), Collins and coworkers[53-56] (Harrick's cell), and Hermans and coworkers[57] (Pike's cell). Based on the design specifications of these cells,[21] the reported modifications, and our recent study of mean residence time distribution in a modified Harrick DR cell,[38] it is very unlikely that any of these reaction cells (with the exception of those with a void volume close to ~1 cm^3 or less) is able to achieve strict rapid exchange of feed gases within a couple of seconds or less at reasonable gas flow rates (<100 cm^3/min). For example, in a modified Spectra Tech cell with a reduced void volume of ~3 cm^3, 90% exchange of gases took ~4.6 s during a transient switch of gases at a flow rate of 80-100 cm^3/min ($\tau_n = V/v \sim 1.8$-2.3 s).[58] Homemade low-volume DR cells are more likely to achieve rapid gas exchanges.[15, 31, 44, 45, 49, 52] Notable examples are the reaction cells reported by Li and Gonzalez[59] (void volume of ~1.2 cm^3, similar to Baiker's[15, 31, 52] and Ferri's[49] design), Schubert et al.[60] (void volume of ~1 cm^3), and Dal Santo et al.[61] (void volume of ~2 cm^3). Despite the low volume of these last two cell designs and that they were made to fit commercial and ubiquitous Harrick Scientific's mirror optics,[21, 38] they are difficult to machine and reproduce and were only tested to temperatures up to 400 °C.

Inspired by the works of Schubert et al.[60] and Dal Santo et al.,[61] here we report the design, fabrication, modelling, and evaluation of a new low void-volume diffuse reflectance cell that is relatively easy to machine, use, and maintain, that can be employed at temperatures as high as ~550 °C, with improved sample temperature monitoring, and that is fully compatible with Harrick Scientific's mirror optics (Praying Mantis™). To study the fluid dynamics of the new DR cell, residence time distribution analyses via pulse experiments and computational fluid dynamic modelling are also reported. To demonstrate its utility, ME-PSD-DRIFTS experiments during ethanol dehydration on a γ-Al_2O_3 catalyst were carried out at similar gas residence and spectroscopic sampling times. We expect this cell design will inspire and contribute to the catalysis community to further our understanding of surface reaction intermediates via transient experiments and to popularize advanced phase sensitive detection techniques such as those described in this work.

2. Experimental

2.1. Cell design and construction

Fig. 1 shows a schematic cut off view of the new low void-volume in situ diffuse reflectance (DR) reaction cell. It was designed to resemble Harrick's HVC high temperature reaction chamber and to fit Harrick's mirror optics (Praying Mantis™). To facilitate machining and allow for flexible choice of materials of construction, it was designed in two main parts: a main cell body (9 in Fig. 1) and a cell housing (7 in Fig. 1). The cylindrical-like cell body was made of corrosion-resistant 316/316L stainless steel (SS) (McMaster-Carr, P/N 89325K56) with the largest outer diameter (OD) being 1.75" and the smallest OD being 0.75". A bridge between these two cylindrical sections was made 3/8" thin to minimize external heat losses due to conduction from the sample cell to the surroundings. The cell body sits on a cell housing made of aluminium (7 in Fig. 1) and is held in place by two retaining plates (13 in Fig. 1) similar to those in Harrick's HVC cell. The top part of the cell body is equipped with a high-temperature ceramic ring (10 in Fig. 1) (McMaster-Carr, P/N 8489K243) to minimize void volume and heat losses from the sample cup, cell body, and reduce dome exposure to high temperatures. A silicon O-ring (McMaster-Carr, P/N 8333T134) provides a seal between the cell body and the IR dome. The dome (11 in Fig. 1) is made of a metallic frame (1.5" OD) with a monolithic ZnSe window (which is a special Harrick's fabrication part) that has a bottom small semi-sphere (1 cm ID) providing minimum void volume (~0.5 cm^3) above the sample cup (0.25" ID x 0.11" H). The sample cup wall is 0.094" thick to provide enough space for an inlet feed (1 in Fig. 1) orifice (1 mm ID) and a well (16 in Fig. 1) on the opposite side to fit a 1/32" external thermocouple (5 in Fig. 1) (Omega, P/N KMQXL-032G-6). Gas feed flows down the sample cup (15 in Fig. 1) via a 2 mm ID orifice. Both inlet and outlet orifices are machined to join 1/8" SS tubing at a 45-degree angle with respect to the sample horizontal plane. The tubing can be attached to the cell body via silver soldering or spot welding. The former is easily accessible and affordable, but limits cell external temperature operation to ~650 °C depending on the silver alloy melting point. At this high limit temperature, as shown later, the actual maximum sample temperature (usually ~100 °C lower than the cell external temperature) will be a function of the carrier gas type and flow rate.[38] With spot welding, although not as common and more expensive, the maximum operating temperature for the reaction cell body can be further increased. Heat to the sample is provided via two external cartridge heaters (4 in Fig. 1) (0.25" x 1.25", 24 V, 100 W, Harrick Scientific) which can be controlled via a homemade temperature controller with cascade control capabilities by receiving feedback from the sample (6 in Fig. 1) (Omega, P/N KMQXL-032G-12) and the external cell (5 in Fig. 1) thermocouples. Note that Harrick's ATC-024-3 temperature controller does not support high temperature operation with two (24 V, 100 W) cartridge heaters. To measure the sample temperature (just under the sample surface, see 15 in Fig. 1), a sample thermocouple (6 in Fig. 1) is inserted in the catalyst bed via the outlet tubing and thorough a metal screen holding the catalyst powder (made from SS 316 mesh, 38 µm opening, McMaster-Carr P/N 9319T189). A similar procedure was reported with a modified Harrick's cell for use with UV-vis DR fiber optics probes.[38]

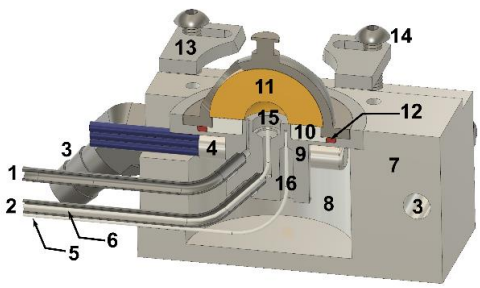

Fig. 1. Cut off view of the low void-volume DRIFTS reaction cell. 1) Gas inlet; 2) gas outlet; 3) cooling port; 4) cartridge heater; 5) external reaction cell body thermocouple; 6) sample thermocouple; 7) reaction cell housing; 8) insulating void space; 9) reaction cell body; 10) insulating ceramic ring; 11) infrared ZnSe dome; 12) O-ring; 13) retaining plates; 14) retaining plate screw; 15) sample cup; 16) external thermocouple well.

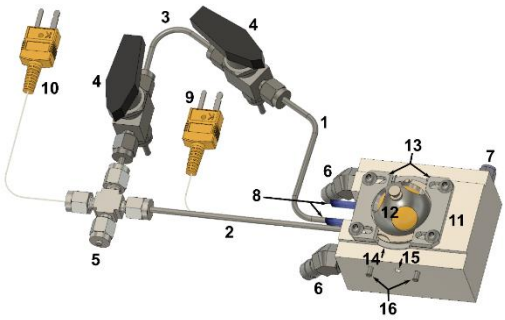

Fig. 2. Top view of the low void-volume DRIFTS reaction cell with accessories. 1) Gas inlet; 2) gas outlet; 3) bypass line; 4) bypass valve; 5) cell backflow port; 6) cooling port; 7) cooling hole plug; 8) cartridge heater; 9) external reaction cell body thermocouple; 10) sample thermocouple; 11) reaction cell housing; 12) infrared ZnSe dome; 13) retaining plates; 14) reaction cell body; 15) mounting hole; 16) dowel mounting pins.

Fig. 2 shows the top view of the reaction cell as it is integrated with a simple bypass flow line via two 3-way SS 1/8" valves (4 in Fig. 2) (Swagelok, SS-41GXS2). A 1/8" SS cross (5 in Fig. 2) (Swagelok, SS-200-4) is installed in the outlet line (2 in Fig. 2) to provide a port for inserting the sample thermocouple (10 in Fig. 2) and a port for back purging and air flushing the outlet line in the case that catalyst sample leaks through the supporting mesh. To hold the sample thermocouple in the cross port, a 1/32" adapter (Valco VICI, EZRF2.5V-5) was employed. A water cooling jacket keeps the external cell housing temperature cooled via holes drilled from front and side ports (6 and 7 in Fig. 2). A SS pipe plug (Swagelok, 1/16", SS-1-P) that was cut to about half its original threaded length was used to plug the cooling side hole (7 in Fig. 2) while two brass 45° elbows (Anderson Metals, 3/8" barb x 1/8" male pipe, P/N 07045-0602) (6 in Fig. 2) were installed in the front cooling holes. An isotemp programmable refrigerated recirculating bath (Fisher Scientific, Model 4100 R20) set at 4 °C pumps coolant to maintain the external housing temperature low and prevent overheating of the sealing O-ring between the dome and the cell body.

2.2. Peripheral setup

Fig. 3 shows the in situ and operando diffuse reflectance infrared Fourier transform spectroscopy (DRIFTS) experimental

setup. It is composed of three main sections: 1) a gas feed system; 2) the low void-volume DRIFTS cell; and 3) the gas phase analysis instrument (Pfeiffer, OmniStar GSD 320 O mass spectrometer, MS). All lines are composed of 1/8" SS tubing. The gas feed system consists of three mass flow controllers (MFC) (Omega, FMA-7103E) and a secondary electronics control module (Brooks, 0154) for the delivery of constant gas flow of gases to the DRIFTS cell. The MFCs were calibrated for flow of He (UHP, Matheson) and Ar (UHP, Matheson). All gas outlets are provided with moisture (Matheson, 450 B series, type 451), oxygen (Perkin Elmer, P/N N9301179), and hydrocarbon (Matheson, 450B series, type 454) traps. Liquid can be fed to the system via a syringe pump (New Era Pump Systems, Inc., NE-8000X2) and Hamilton's gas tight syringes through an online ultra-Torr fitting (Swagelok, SS-4-UT-1-2) attached to a SS tee (Swagelok, SS-200-3TTF) provided with a high temperature septum (Restek, P/N 27090). Injection port and lines all throughout the reaction cell and MS were heated to about 80-100 °C to prevent liquid condensation during concentration modulation of ethanol dehydration experiments as described later. For ethanol modulation experiments, a 6-port 2-position valve (6WV) (VICI, 1/16" fittings, 0.40 mm, equipped with a medium temperature Valcon E rotor, 400 psi, 225 °C) is switched with a high speed and low torque (VICI, EHMA) microelectric actuator to change periodically the feed flow from a Feed 1 gas mixture (containing ethanol) to a Feed 2 (see Fig. 3) inert gas mixture. A 6WV was employed instead of a 4WV to also allow use in pulse experiments such as those previously reported to determine cell's average residence time.[38] The low void-volume cell was designed to resemble in size the Harrick Scientific's HVC reaction cell and, therefore, be compatible with Harrick's Praying Mantis™ mirror optics. The combined cell + mirror optics were placed in the sample compartment of an FTIR spectrometer (Vector 70, Bruker) equipped with a mercury-cadmium-telluride detector (MCT D316/BP) and with rapid scan capabilities required for ME spectroscopy experiments.

2.3 Reaction cell residence time distribution properties and computational fluid dynamics

Analysis of the cell's residence time distribution (RTD) was performed via recently reported pulse techniques[38] that use the E(t) curve composed of normalized (to a total area of 1) concentration data.[62, 63] Briefly, the reaction system is modified such that it is provided with a 50 µL sample loop in a 6WV for

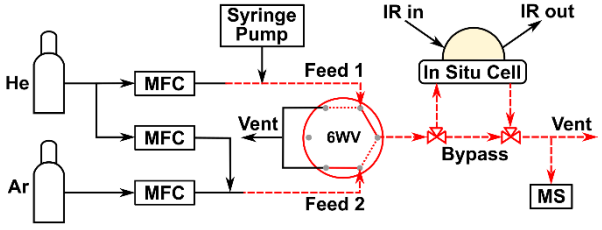

Fig. 3. Schematics of the in situ low void-volume diffuse reflectance IR cell and experimental setup. MFC = mass flow controller; MS = mass spectrometer; IR = infrared light; 6WV = 6-port two-position switching valve. Dashed lines and red color indicate that transfer lines (and 6WV) are heated to avoid possible condensation of liquid injected via the syringe pump. 6WV can switch to two positions (dotted and solid lines).

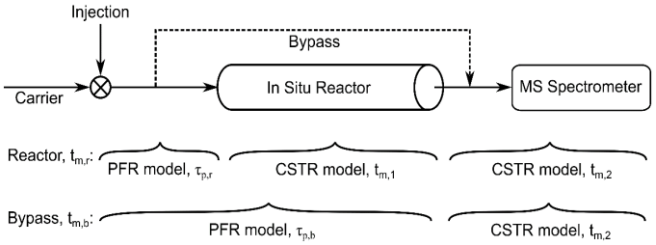

Fig. 4. Residence time distribution models for estimation of in situ reaction cell mean residence time (MRT). Here, $t_{m,r}$ and $\tau_{p,r}$ are the overall and plug flow reactor (PFR) model MRT for transfer lines to cell, respectively, resulting from flow through the reaction cell, whereas $t_{m,b}$ and $\tau_{p,b}$ are the overall and PFR model MRT for transfer lines to MS, respectively, when the gas bypasses the reaction cell (dashed line); and $t_{m,1}$ and $t_{m,2}$ are the in situ reaction cell and MS detection chamber MRTs, respectively. (Reprinted from ref. 38: P.D. Srinivasan, S.R. Nitz, K.J. Stephens, E. Atchison, and J.J. Bravo-Suarez, Appl. Catal. A: Gen., 2018, 561, 7-18, Copyright © 2018, with permission from Elsevier).

pulse experiments with Ar, CO_2, H_2, and O_2 and He as the carrier gas (more details of a related system are provided in reference 38). The system setup transfer lines from the point of the gas pulse injection (with carrier flow rate of 45 cm^3/min) to the reaction cell and to the MS were considered as a series of plug flow and continuously-stirred tank reactors (PFR and CSTR) as shown schematically in Fig. 4. The method also requires gas pulse measurements via a line that bypasses the reactor such as that shown in Figs. 2, 3, and 4, which in combination with pulses through the reaction cell allows estimation of the average residence time of the pulsed gases in the system components. Additionally, the reaction cell's E(t) signal is modelled as two reactors in series, one for the in situ cell and the second for the MS chamber. From the best fit of various model combinations, the fluid behaviour of the reaction cell can be inferred.

To further gain insights into the fluid behaviour within the reaction cell, a computational fluid dynamic simulation with He flow (45 and 180 stp cm^3/min) under isothermal conditions (25 °C) was performed based on the corresponding Navier-Stokes equations:[64]

$$\frac{\partial \rho}{\partial t} + \nabla \cdot \rho \mathbf{v} = 0 \quad (1)$$

$$\rho\left(\frac{\partial \mathbf{v}}{\partial t} + \mathbf{v} \cdot \nabla \mathbf{v}\right) = -\nabla p + \mu \nabla^2 \mathbf{v} + \rho \mathbf{g} \quad (2)$$

These equations were solved using a finite element approach with a segregated solver by setting a desired flow rate at the inlet tube and a pressure of zero at the outlet tube. Lastly, the reaction cell 3D model shown in Fig. 1 was created by Autodesk® Fusion 360 and the numerical simulations were performed with Autodesk® CFD 2018.

2.4. In situ diffuse reflectance cell operation

The in situ and operando spectroscopic characterization of solid catalysts is commonly made by diffuse reflectance spectroscopy because: 1) it can be applied to a wide range of solid materials with high absorption and scattering properties; 2) it does not require sample preparation; 3) sample can be recycled; and 4) sample holder resembles the operation in fixed bed reactors.[21] For proper operation of the diffuse reflectance spectroscopic cell, some basic conditions must be met including: 1) sample thickness of at least 2 mm and 2) fine powders, usually in the

~5-50 µm range. The depth of the sample in the reaction cell is 2.8 mm and particle sizes of ~38-75 µm are used which meet these suggested conditions.[21] For operation of the cell, usually about 40-75 mg of catalyst sample are loaded into the cell. Unlike transmission spectroscopy where sample needs to be pelletized or pressed in special grids, no special sample treatment is needed for in diffuse reflectance experiments, except those required afterwards for best practices before reaction testing (e.g., high temperature pretreatment in O_2, H_2, etc.) or for initiating spectroscopic measurements (e.g., blank, reference measurements, etc).[21]

2.5. Modulation excitation spectroscopy with phase sensitive detection (MES-PSD)

As a preamble to MES-PSD, let us recall that periodic functions are amenable to Fourier transform (FT) analysis, where data (or spectra) in the time domain are converted into the frequency domain upon Fourier transformation.[65] A classic example of such transformation is that in acoustic signal processing where a sound can be split into its frequency components by FT. Once in the frequency domain, undesirable frequencies (e.g., of noise) can be easily removed, and a cleaner sound is then produced upon application of the inverse FT (IFT).[66] Mathematically, $X(\omega)$ is the (complex) FT of the function x(t):

$$X(\omega) = \frac{1}{2\pi}\int_{-\infty}^{\infty} x(t)e^{-i\omega t}dt \quad (3)$$

And x(t) can be recovered from $X(\omega)$ by the IFT equation (to the so-called phase domain):

$$x(t) = \int_{-\infty}^{\infty} X(\omega)e^{i\omega t}d\omega \quad (4)$$

Where ω is the frequency.

In the in situ IR spectroscopic characterization of solid catalysts, the IR spectra are often populated by many bands which are associated to background, baseline shift, noise, spectator species, accumulating species, slow reacting species, and true reaction intermediates. Discriminating the latter is a difficult and complex task as the population and, therefore, intensity of these species is small. In analogy with the sound example above and similar to the analysis of small signals in the presence of a large noise via a phase-sensitive detection (PSD or also called demodulation) method using a lock-in amplifier,[67, 68] FT could be used to discriminate fast reacting intermediate species from spectators and slow reacting species. However, to do so, a periodicity must be induced in the reaction system. This is the purpose of introducing a periodic feed modulation of frequency ω, as intermediate species participating in elementary steps of a catalytic cycle should respond at a similar frequency, whereas slow and spectator species will not. The goal is then to force surface species to be periodic at frequencies in the range of reaction turnover frequencies to capture information of intermediate species. For the processing of infrared spectra, Baurecht and Fringeli[14] developed a numerical method to carry out a combined FT + IFT (PSD) procedure by solving the following equation:

$$A_k^{\phi_k^{PSD}}(\tilde{\nu}) = \frac{2}{\mathrm{T}}\int_{\mathrm{o}}^{\mathrm{T}} A(\tilde{\nu},t)\sin(k\omega t + \phi_k^{PSD})dt \quad (3)$$

Where $A_k^{\phi_k^{PSD}}(\tilde{\nu})$ is referred to as the phase-resolved absorbance spectrum or IFT (phase-domain response) of the periodic time dependent absorbance $A(\tilde{\nu},t)$ (time-domain response), T is the time length of one period, ω is the modulation frequency, k is a positive integer (where k=1 is the fundamental frequency, and $k>1$ are the corresponding frequency harmonics),[34] and ϕ_k^{PSD} is the demodulation phase angle.[13] Depending on the shape of the periodic feed wave(e.g., sine, square, triangle, sawtooth, etc), it is possible to have in the same experiment higher frequency harmonics (k>1) that could be used for deriving information of faster reacting (short-lived) species.[34] Irrespective of the modulation waveform, in the method described above we are mainly concerned with the most dominant ω component (k=1), that is, when the spectroscopic signal responds at the same feed modulation frequency. Details on the numerical method and technique[13, 14] and a review of its application in catalysis[12] have been previously reported. Here, we have implemented a similar PSD (FT + IFT) procedure via a homemade Python (www.python.org) software code for processing of the infrared spectra collected during feed concentration modulation.

2.6. Modulation experiment

To evaluate the performance of the new low void-volume reaction cell for transient catalytic studies, ethanol dehydration on a γ-Al_2O_3 at 200 °C was used as an example of application of MES-PSD to FTIR data. In a typical experiment, ~45 mg of (38-75 µm) γ-Al_2O_3 (SBa200, Sasol, BET surface area = 189 m^2/g) were loaded to the reaction cell (Fig. 1). During the modulation experiment, Feed 1 (Fig. 3) consisted of ~1 kPa ethanol, which was introduced via a syringe pump (60 µL/h of liquid ethanol at ambient temperature) and carried by 40 std (ambient T and P) cm^3/min of He for a total flow rate of approximately 40.4 std cm^3/min. All transfer lines were heated to about 80-90 °C via wrapped heating tapes (HTS Amptek, 4' x 208 W, 120 V, P/N AWH-051-040DM-MP), insulated with silica tape (AVS Industries, P/N WT36CH-1), and controlled via variable transformers (Circuit Specialists, P/N TDGC2-0.5). Feed 2 consisted of a mixture of Ar/He = (10.4 std cm^3/min)/(30 std cm^3/min), where Ar can be used as internal standard for mass spectrometry data. Prior to cell loading, catalyst was calcined ex situ in a muffle furnace (Thermo Scientific, Thermolyne 48025-60-80) in static air at 350 °C (5 °C/min) for 2 h. Once in the cell, the catalyst was heated in He flow (45 std cm^3/min, Feed 2) to 200 °C. Feed concentration modulation was then started by switching periodically between Feed 2 and Feed 1 flows every 45 s (via a LabVIEW 2018 VI program routine) to yield a period of 90 s. This results in a frequency that falls within the range of typical reaction TOFs (ω = 1/90 = 0.0111 Hz). A total of 15 periods were repeated. Once feed modulation starts, IR spectra are also collected simultaneously via rapid scan, about every 1 s (16 scans, 4 cm^{-1}) to match the average gas residence in the reaction cell (~ 1 s).

3. RESULTS AND DISCUSSION

3.1. Cell design

The work reported here arose from the lack of commercial in situ diffuse reflectance (DR) reaction cells that provide a low void-volume required for transient spectroscopic experiments to discriminate surface reaction intermediates.[21] One of the most ubiquitous DR cells/optical system is that of Harrick Scientific, perhaps due to its flexibility for use with UV-visible, FTIR, or Raman spectroscopic just by changing to compatible window materials.[21, 38] This DR cell, just like other commercial cells, possesses significant void volumes that prevent rapid exchange of gases needed in dynamic reaction experiments. A recent report suggested that average residence times of less than a couple seconds (similar to those found in transmission cells)[21] could be achievedin a modified Harrick' cell, but at unreasonably high gas flow rates (e.g., >200 cm^3/min).[38] A new low void-volume reaction cell would be, then, highly desirable. Schubert et al. [60] (void volume of ~1 cm^3), and Dal Santo et al.[61] (void volume of ~2 cm^3) reported cell designs that could be compatible with Harrick's mirror optics. While these cells achieved the goal of reducing the void volume, they lack sufficient design details or require a complex machining process for their fabrication, which makes them difficult to reproduce. Inspired by these designs and addressing their drawbacks, we now report a new low void-volume DR cell in Fig. 1. The main goal was to make a cell that was relatively simple to machine and reproducible in most catalysis laboratories with machining capabilities, that was compatible with commercial mirror optics (e.g., Harrick's Praying Mantis™) and parts (e.g., Harrick's low void-volume ZnSe hemispherical window/dome, cartridge heaters), and that could be easily adapted to UV-visible, FTIR, and Raman spectroscopies.[21, 38] This cell features a low void-volume (~1.0 cm^3) mainly arising from the volume of the window's empty space above the sample (~0.5 cm^3) and that of the inlet and outlet tubing (1 and 2 in Fig. 2). Additionally, the use of cartridge heaters simplifies operation and facilitates parts replacement when needed. Additional characteristics relevant for transient operation will be described in subsequent sections, whereas additional suggestions for cell operation and improvements (Section S1) and machining blueprints (Figs. S1-S5) are provided as supporting material.

3.2. Residence time distribution and cell fluid flow dynamics

The reaction cell system (Fig. 3) could be considered as a combination of a series of ideal PFR and CSTR reactors encompassing transfer lines, reaction cell, and MS chamber. Such an arrangement proved to be useful to estimate the average residence time in Harrick's reaction cell.[38] Following a similar method via experimental gas pulses and residence time distribution methods,[62, 63] it was possible to obtain the mean residence time (MRT) in the new reaction cell. Comparison of the normalized composition (E(t) function) of an Ar pulse through the bypass line with that one through the reaction cell (Fig. S6) shows that they are similar in size, although that of the former is slightly sharper indicating a minor contribution to the cell's RTD due to void volume. This is in contrast with the results for Harrick's cell showing significant differences in size and

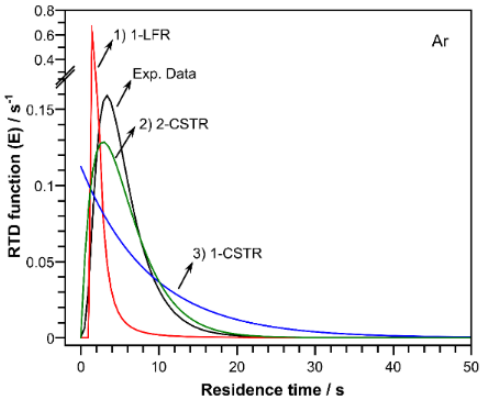

Fig. 5. Residence time distribution (RTD) profiles of Ar gas pulse through the reaction cell and corresponding fitted RTD reactor models: one laminar flow reactor (1-LFR, trace 1), two continuous-stirred tank reactors of same volume (2-CSTR, trace 2), and one CSTR (1-CSTR, trace 3). Experimental residence time distribution data were offset to zero by the corresponding $\tau_{p,r}$. Conditions: ambient temperature, 1 atm, 50 µL loop, He carrier flow of 45 std cm^3/min.

shape for the RTD function because of Harrick's cell larger void volume.[38]

Results for the overall, in situ cell, and MS chamber's MRT for different gases as well as the space time of transfer lines are shown in Table 1. Several observations can be made: 1) the overall MRTs for all gases were fairly similar despite significant differences in the diffusion coefficients of all gases indicating that mass transfer is controlled by convection and bulk transport rather than by diffusion; 2) the time required for detection of 90% of the pulsed gases (~17.6 s) was significantly shorter than that reported for Harrick's unmodified cell (~64.5 s);[38] and 3) while the residence times $\tau_{p,r}$, $\tau_{p,b}$, and $t_{m,2}$ are unique to the specific reaction system configuration, $t_{m,1}$ represents the average residence time in the reaction cell. At a gas flow rate of 45 cm^3/min, the average $t_{m,1}$ was 1.3 s. This is a significant improvement over the unmodified and modified (reduced volume) Harrick's cell of 21.2 and 12.7 s at identical pulse conditions. These results clearly demonstrate that the cell reported here can achieve rapid gas exchanges (within about 1-1.5 s) at moderate gas flow rates.

Table 1. Residence time distribution of various gases in the in situ reaction system with the low void-volume reaction cell

Gas	$t_{m,r}$ (σ) (s)	t $RTD_{90\%}$ (s)	$\tau_{p,r}$ (s)	$\tau_{p,b}$ (s)	$t_{m,1}$ (s)	$t_{m,2}$ (s)
Ar	12.7 (3.1)	17.1	6.5	5.3	1.4	5.0
CO_2	12.7 (3.4)	18.4	6.0	5.1	1.5	5.2
H_2	12.3 (2.7)	17.0	7.7	5.5	0.8	3.9
O_2	13.7 (3.3)	17.9	7.2	5.3	1.5	5.0
Average	12.8	17.6	6.9	5.3	1.3	4.8

$t_{m,r}$ = mean residence time of pulse gas to reach MS detector (via in situ reaction cell), σ = standard deviation, t RTD90% = residence time required for 90% of the pulse gas to reach the MS detector, $\tau_{p,r}$ = space time for a plug flow reactor: tubing line before in situ reaction cell, $\tau_{p,b}$ = space time for a plug flow reactor: tubing line bypassing in situ reaction cell, $t_{m,1}$ = mean residence time of pulse gas through in situ reactor based on an ideal CSTR, $t_{m,2}$ = mean residence time of pulse gas in mass spectrometer before reaching detector based on an ideal CSTR. Experimental conditions: He carrier 45 cm^3/min, 50 µL gas pulse, 1 atm, 25 °C.

It has been previously reported that the flow dynamics of Harrick's cell can be approximated by a CSTR RTD model.[38] To check the dynamics of the low void-volume cell, the E(t)

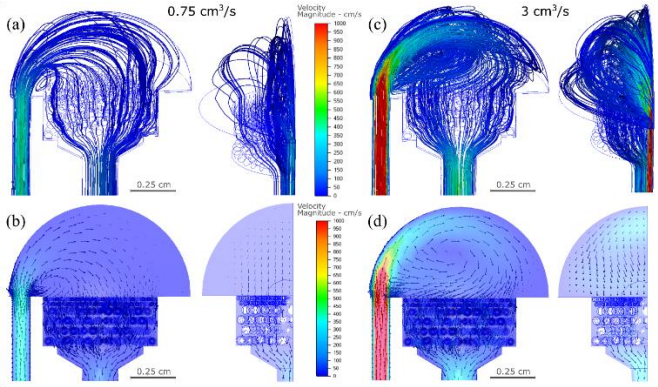

Fig. 6. Reaction CFD simulation of velocity magnitude (in cm/s): (a, c) particle trace and (b, d) cutting plane views. Conditions: He gas, 25 ºC, outlet pressure (gauge) of 0 Pa, and volumetric flow to cell of: (a, b) 45 cm³/min and (c, d) 180 cm³/min. Left figure: right side view (with respect to flow inlet) of vertical plane at cell center point; right figure: front view (with respect to flow inlet) of vertical plane at cell center point. Catalyst bed was modelled by loosely packed spheres of 240 (two top layers) and 500 µm (bottom 4 layers).

function of an Ar pulse was fitted to several ideal models including a laminar flow reactor, a CSTR, and a two CSTR in series model as shown in Fig. 5. The results indicate, as expected, that the RTD function is better described by a two-ideal reactor model (of equal volume) because of additional gas mixing in the MS chamber. The lack of fitting around the function maximum suggests that perhaps a LFR + CSTR series model may be a better representation of the flow dynamics. However, such model did not result in a better fit (Fig. S7, Section S2) indicating that the reaction cell fluid dynamics likely has a complex flow distribution with contributions from both LFR and CSTR.[69]

To further evaluate the flow dynamics within the reaction cell, a CFD modelling study was performed as presented in Fig. 6. The results show flow stream lines as gas enters the reaction cell space above, through, and past the catalyst bed. At 45 cm³/min of inlet flow rate (Fig. 6a), the average velocity magnitude is fairly constant and relatively low (<50 cm/s) in the volume above the catalyst bed. The gas flow followed variable and, in some cases, random paths with mixing occurring towards the feed entrance. Increasing the entrance flow rate to 180 cm³/min (Fig. 6c) further highlighted the cell complex flow path with laminar flow velocities, but random mixing above the catalyst. This simulation confirmed our assertions of complex gas hydrodynamics within the cell that could be better described by a hybrid LFR/CSTR model.[69] Such approach, however, was not attempted here. For simplicity and due to fair fitting to RTD data in Fig. 5 with 2-CSTR in series, a CSTR model was kept for cell's RTD calculations.

Figs. 6b and 6d show that the flow path also distribute over the entire catalyst bed, which ensures a relatively uniform sample coverage during spectroscopic measurements. Additionally, small zones of stagnant gas could be identified along the rim of the sample cup. While a more distributed feed could minimize the presence of these stagnant gas zones, it is not clear that such modifications are justified given the small cell volume and rapid exchange of gases, as indicated by the symmetric RTD curve describing the flow pattern. CFD simulations in absence of the catalyst bed (Fig. S8) showed a different hydrodynamic behaviour within the reaction cell, highlighting the risks modelling reaction cells without catalyst particles.

3.3. Reaction cell temperature gradients

The temperatures in the reaction cell were monitored via two thermocouples. One was in direct contact with the sample to track the catalyst temperature while the second one monitored the external wall of the sample cup. In DR reaction cells it has been recognized that temperature differences exist and that are accentuated by heat losses via radiative, conductive, or convective transport.[35, 38, 39, 70] Fig. 7 shows the correlation between the catalyst and external sample cup temperatures. At all conditions there are temperature differences that increase with an increase in the reaction cell temperature. Such differences could be as high as 120 °C in He flow as the catalyst approaches 500 °C. In general, it is noted that gases whose heat capacity is relatively high such as He (C_p = 1.25 Btu/lbmol/F) will tend to facilitate heat transport and losses more than those seen with Ar (C_p = 0.12 Btu/lbmol/F). Also, heat transport is more efficient under gas flowing conditions. These trends follow those by Harrick's cell where maximum sample temperatures of about 500 °C are achieved at low flow rates of Ar. Because of the more compact nature of the low void volume cell, it appears that heat loses are slightly larger than those previously reported for Harrick's. This suggests that further improvements to sample heating design could help increase heat transport by minimizing heat losses. Designs such as those by Dal Santo et al.[61] with a vertically oriented dual cartridge or via a coiled heating system[60] may be worth exploring. In the present cell, sample temperatures above 550 °C were not attempted to avoid possible issues with the inlet and outlet tubing because they were attached to the reaction cell body by silver soldering. Overall, the cell performed well over a wide range of temperatures of relevance for most gas-solid catalytic applications.

3.4. Application to ME-PSD-DRIFTS

In this section, we demonstrate the application of the new low void-volume DR cell for the in situ IR spectroscopic study of

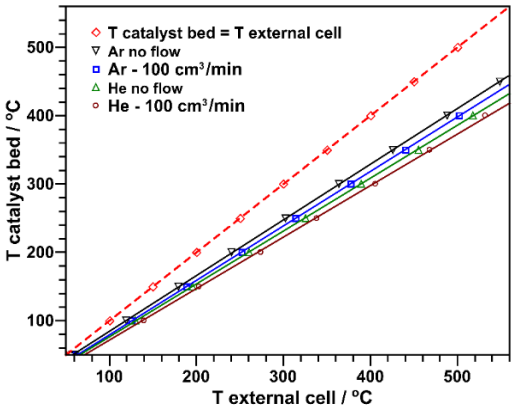

Fig. 7. Relation between temperature of catalyst bed and temperature of external reaction cell. Sample is an amorphous low surface area purified silica (< 125 µm).

ethanol dehydration on a commercial γ-Al_2O_3 (SBa200, Sasol) at 200 °C via feed modulation excitation-phase sensitive detection-diffuse reflectance infrared Fourier transform spectroscopy (ME-PSD-DRIFTS). Reactivity tests in a fixed bed reactor (200 °C, 1 kPa EtOH, total gas flow rate ≈ 80 cm^3/min, catalyst weight = 76 mg) showed that this catalyst formed predominantly diethyl ether (5.9 mmol/g_{cat}/h) and ethylene to a lesser extent (0.2 mmol/g_{cat}/h). Acidity in this catalyst is mainly due to Lewis acid sites (408 µmol/g), as determined from TPD of adsorbed pyridine followed by FTIR (not shown), which is expected for γ-Al_2O_3 materials. This agrees with prior reports on this catalyst's performance at low temperatures.[71, 72] Additional catalyst characterization and catalytic performance can be found elsewhere.[73] In situ ME-PSD-DRIFTS were performed at similar space velocity and ethanol partial pressure (200 °C, high concentration during modulation = 1 kPa EtOH, total gas flow rate ≈ 45 cm^3/min, catalyst weight ≈ 45 mg). At the total gas flow rate of 45 cm^3/min, it was shown in Section 3.2 that the mean residence time of gases was approximately 1.3 s, whereas the sampling frequency was ~1.0 Hz (sample/s) ensuring the matching of gas phase exchange time scale with that of the spectroscopy sampling. Additionally, the 1 Hz sampling frequency ensures a high enough frequency to satisfy the Nyquist sampling criterion for Fourier transform analysis. If we conservatively assume that the highest harmonic of the fundamental frequency is 10ω (k = 10), then, a minimum sampling rate of twice that value (0.222 Hz) would be required to reconstruct the original time-dependent absorbance function, which is satisfied in this work. During the feed modulation experiment, two feed lines with identical total flow rates (total flow rate = 45 cm^3/min, Feed 1: EtOH/He ~ 1/100 and Feed 2: Ar/He ~ 26/75, see Fig. 3) are switched periodically every 45 s to yield one period of 90 s and feed modulation frequency of 1/90 = 0.0111 Hz. Such feed modulation will induce periodic changes on surface intermediate species that can be tracked by in situ FTIR spectroscopy. Online MS tracking of Ar, unreacted ethanol, and reaction products showed that the feed modulation had a square-like waveform and that the catalyst was active in the dehydration of ethanol to diethyl ether and ethylene (Fig. S9).

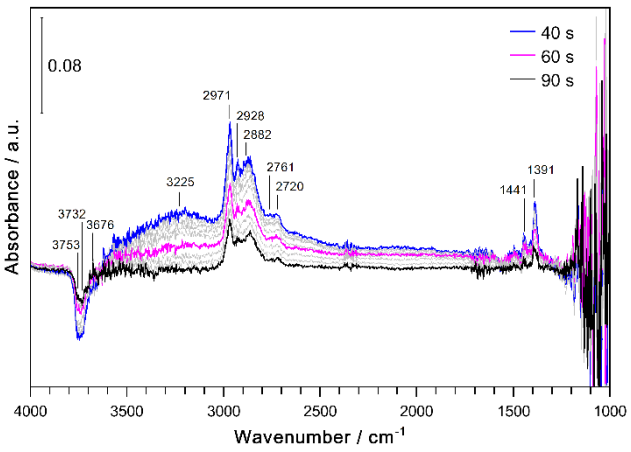

Fig. 8. Time domain difference IR spectra during ethanol dehydration on γ-Al_2O_3. Difference spectra with respect to time zero at low ethanol concentration. Conditions: 200 °C, 1 atm, feed modulation from He/Ar → He+EtOH (1 kPa), modulation frequency = 1/90 Hz, total gas flow ~45 std cm^3/min.

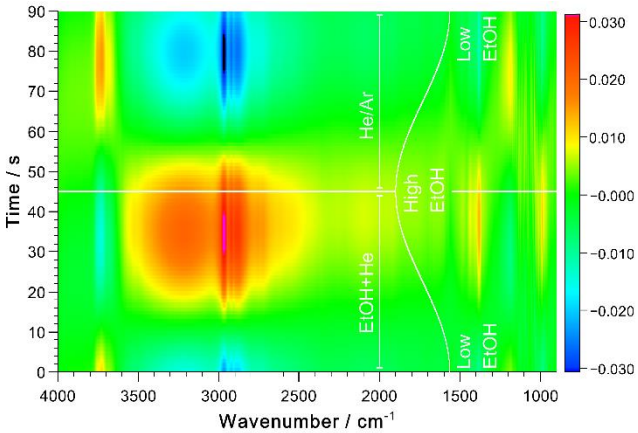

Fig. 9. Contour plot of phase domain in situ diffuse reflectance IR spectra during ethanol (EtOH) dehydration on γ-Al_2O_3. Conditions: 200 ºC, 1 atm, feed modulation from He/Ar → He+EtOH (1 kPa), modulation frequency = 1/90 Hz, total gas flow ~45 std cm^3/min, catalyst weight ~45 mg. EtOH sine wave feed composition curve added to guide the eye.

Fig. 8 presents the difference IR spectra during a feed modulation period of 90 s. This is the classical approach to transient spectra analysis. While this method captures general changes over the whole wavenumber range, the spectra remains somewhat noisy, the discrimination of small peaks is difficult, and trends are challenging to establish. Upon processing the data via PSD, Figs. 9 and 10 were obtained. Fig. 9 shows the contour plot of the phase domain spectra after IFT reconstruction of the periodic time-dependent absorbance including only species that respond to the fundamental modulation frequency ($\omega = 0.0111\ Hz$). Fig. 9 also reflects spectra changes over one modulation period of 90 s as indicated in the Y axis. While the actual modulation waveform is not a sine wave, this has been added to Fig. 9 to guide the eye and to show regions where low and high concentration of ethanol feed are expected. In the current spectra, color differences between blue and red show regions of low and high surface coverage of species with respect to a mid-point in the periodic modulation. This allows rapid visual evaluation for presence of peaks and possible relationship among them. In the present case, a quick observation can be made: at high concentrations of ethanol (between 20-50 s) there is an abundance of surface species in the 2600-3500 cm^{-1} range, which appear to follow an opposite behaviour to those in the 3700-3800 cm^{-1} range. The contour plot during modulation then offers a powerful visual tool to quickly evaluate trends that are not obvious in a time domain difference spectrum. More detailed observations should come from individual spectra at various ethanol compositions or time in the phase domain.

The trace view of Fig. 9 is shown in Fig. 10, which details the temporal changes over the 1000-4000 cm^{-1} wavenumber range for the species that respond to the feed modulation. It is seen that the PSD procedure significantly reduced the noise level and enhanced the signal and definition of weak peaks, not easily discernible in the time domain via difference spectra (Fig. 8). In this case, several bands are noticeable:

1) Bands at 1391 and 1441 cm^{-1} due to undissociated ethanol[74]

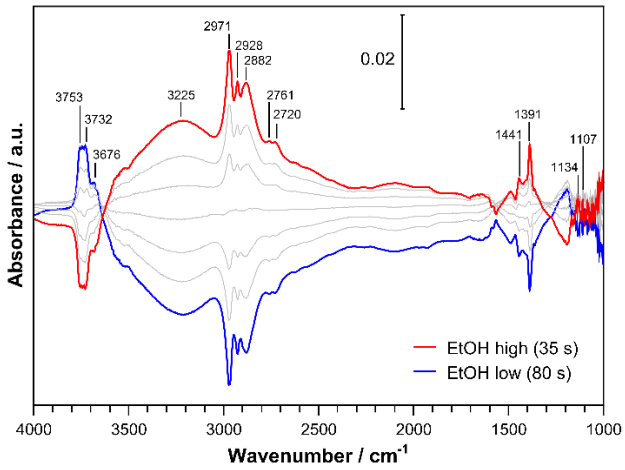

Fig. 10. Phase domain in situ diffuse reflectance IR spectra during ethanol dehydration on γ-Al_2O_3. Conditions: 200 ºC, 1 atm, feed modulation from He/Ar → He+EtOH (1 kPa), modulation frequency = 1/90 Hz, total gas flow ~45 std cm^3/min.

2) Bands at $\nu_s(CH_2)$ = 2882 cm^{-1}, $\nu_s(CH_3)$ = 2928 cm^{-1}, and $\nu_{as}(CH_3)$ = 2971 cm^{-1} due to C-H stretching of adsorbed ethanol[76, 77]
3) A broad large band in the 3100-3500 cm^{-1} range due to the presence of adsorbed water[78] and ethanol dimers[79] and trimers[80]
4) Bands at 3676, 3732, and 3753 cm^{-1} due to various types of surface alumina hydroxyl sites[81-83]

At the reaction conditions of this study (1 kPa EtOH, 200 °C), the predominant product of reaction is diethyl ether as measured in parallel experiments in a fixed bed reactor[73] and expected for γ-Al_2O_3 catalyst.[71, 84] Therefore, the presence of adsorbed ethanol and the absence of bands characteristic of ethoxide or adsorbed diethyl ether (not discernible above the noise level in the 1000-1150 cm^{-1} region, e.g., 1134 and 1107 cm^{-1} due to diethyl ether), is consistent with the conversion of ethanol on γ-Al_2O_3's acid-base site pairs to diethyl ether likely via an SN2 mechanism from an adsorbed ethanol molecule and an incipient alkoxide ion as depicted in Fig. 11.[85]

Additionally, the presence of ethanol and water dimers and trimers is also in agreement with reported inhibited kinetics by these species during ethanol conversion on γ-Al_2O_3.[84] The opposite behaviour observed for various hydroxyl species as ethanol is adsorbed and reacted on the catalyst surface also suggests their involvement in ethanol conversion.[72, 86] The

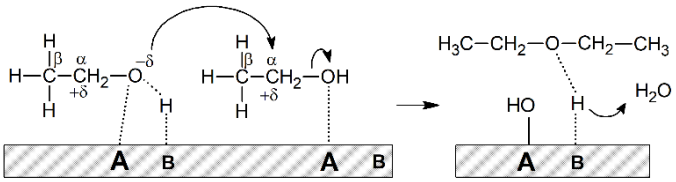

Fig. 11. Ethanol conversion to diethyl ether via an SN2 mechanism. An incipient ethoxide species (left molecule) reacts with an adsorbed ethanol (middle molecule) to form diethyl ether. (Adapted from ref. 85: J.I. Di Cosimo, V.K. Díez, M. Xu, E. Iglesia, C.R. Apesteguía, J. Catal., 1998, 178, 499-510, Copyright © 2018, with permission from Elsevier).

results of Fig. 10 clearly show that several types of hydroxyl species, not just one, are likely active sites for ethanol conversion on γ-Al_2O_3. Although assignments of these peaks remain controversial,[81, 82] they are likely related to type II or type III bridged hydroxyls (3676 cm^{-1}),[81] type I terminal OH attached to penta-[83] or hexacoordinate Al (3732 cm^{-1}), and type I OH attached to octahedrally coordinated Al on (100) plane (3753 cm^{-1}).[82, 83]

In summary, we have shown that a new low void-volume DR reaction cell in combination with ME-PSD-DRIFTS techniques allowed unique access not only to enhanced spectral signals but also to a rigorous assessment of their relations as possible reaction intermediate species at in situ and operando conditions relevant for catalytic conversions. The results shown here highlight the use of a low void-volume DRIFTS cell to allow rapid transient changes (e.g., with frequencies in the order of reaction TOFs) required for the ME-PSD methodology. The information thus attained directly reflects the dynamics of surface species that respond to gas phase periodic changes, however, spectra obtained in the time domain with commercial cells having large dead volumes may still be able to provide information on possible intermediate species with clever experiments and proper reference spectra, when required, as demonstrated by FTIR-SSITKA[6, 7] and transient methods.[9, 10] Even application of ME-PSD-DRIFTS in a cell with significant large dead volume may produce qualitatively valuable information (depending on the chemistry under study and experimental conditions), but will likely preclude quantitative kinetic data analysis because of difficulty in modelling the mixing dynamics within the cell and predicting temporal concentrations above the catalyst sample. Application of large dead-volume DRIFTS cells to ME-PSD also carry the risk of introducing additional complications such as significant gas phase contributions to spectra. The reason for this is the concentration attenuation within the cell's void volume which would require the use of higher feed concentration differences than those required in a low dead-volume cell to induce measurable periodic changes on surface species.

In the application of MES-PSD-DRIFTS technique, it is also worth cautioning that the detection of surface species that respond to modulation frequency does not ensure they are true surface reaction intermediates. For this purpose, additional spectrokinetic methods should be employed to demonstrate that the (conversion or formation) reaction rate of surface species is within the same order of magnitude of the conversion rate measured online or in experiments in a bench scale reactor.[6, 9-11]

4. Conclusions

In this work, we have developed a new low void-volume reaction cell for in situ and operando diffuse reflectance infrared spectroscopic studies of solid catalysts. The cell is compatible with Harrick Scientific's mirror optics (Praying Mantis™) and could be easily adapted for use with UV-visible and Raman spectroscopies by appropriate dome/window changes. It was demonstrated by residence time distribution pulse experiments and computational fluid dynamic (CFD) simulation that the reaction cell flow dynamics possessed elements of laminar flow and CSTR reactors, but that it could be

fairly described as an ideal CSTR. The reaction cell presented mean residence times of about 1.3 s at moderate gas flow rates of 45 cm^3/min, which matched the time scale for spectra sampling. This new reaction cell enabled the implementation of a phase sensitive detection (PSD) procedure (Fourier Transform + Inverse Fourier Transform) for periodic gas feed changes (concentration modulation excitation) of in situ infrared spectroscopy data during ethanol dehydration at 200 °C on γ-Al_2O_3. It was demonstrated that the new cell and PSD technique allowed the identification of likely surface reaction intermediates that conform with ethanol conversion to diethyl ether likely via an SN2 mechanism. Additionally, several alumina hydroxyl species were also identified as possible active species. Overall, the authors hope that this work can contribute to the catalysis community by providing characterization tools that can be easily reproduced and implemented as well as non-conventional methods that can help discriminate reaction intermediates in catalytic cycles for numerous gas-solid phase reactions.

Conflicts of interest

There are no conflicts to declare.

Acknowledgements

Acknowledgment is made to the Donors of the American Chemical Society Petroleum Research Fund for support of this research, grant No 58044-DNI5. The authors also acknowledge financial support by the National Science Foundation, grant No OIA-1539105 and to the University of Kansas through the New Faculty General Research Fund award #2302093.

References

1 F.C. Meunier, *Chem. Soc. Rev.*, 2010, **39**, 4602-4614.
2 N.E. Tsakoumis, A.P.E. York, D. Chen, M. Ronning, *Catal. Sci. Technol.*, 2015, **5**, 4859-4883.
3 B.M. Weckhuysen, *Chem. Commun. (Cambridge, U. K.)*, 2002, 97-110.
4 B.M. Weckhuysen, *Phys. Chem. Chem. Phys.*, 2003, **5**, 4351-4360.
5 S.L. Shannon, J.G. Goodwin, *Chem. Rev. (Washington, DC, U. S.)*, 1995, **95**, 677-695.
6 F.C. Meunier, *Catal. Today*, 2010, **155**, 164-171.
7 C.M. Kalamaras, S. Americanou, A.M. Efstathiou, *J. Catal.*, 2011, **279**, 287-300.
8 E.V. Kondratenko, *Catal. Today*, 2010, **157**, 16-23.
9 T. Gott, S.T. Oyama, *J. Catal.*, 2009, **263**, 359-371.
10 J.J. Bravo-Suárez, K.K. Bando, J.I. Lu, M. Haruta, T. Fujitani, S.T. Oyama, *J. Phys. Chem. C*, 2008, **112**, 1115-1123.
11 S.T. Oyama, W. Li, *Top. Catal.*, 1999, **8**, 75-80.
12 P. Müller, I. Hermans, *Ind. Eng. Chem. Res.*, 2017, **56**, 1123-1136.
13 A. Urakawa, T. Bürgi, A. Baiker, *Chem. Eng. Sci.*, 2008, **63**, 4902-4909.
14 D. Baurecht, U.P. Fringeli, *Rev. Sci. Instrum.*, 2001, **72**, 3782-3792.
15 N. Maeda, F. Meemken, K. Hungerbühler, A. Baiker, *ACS Catal.*, 2013, **3**, 219-223.
16 B.M. Weckhuysen (Ed.), In: *In-Situ Spectroscopy of Catalysts*, American Scientific Publishers, Stevenson Ranch, CA, 2004, pp. 1-332
17 J.F. Haw, In-Situ Spectroscopy in Heterogeneous Catalysis, Wiley-VCH, Weinheim, Germany, 2002, pp. 1-276.
18 J.J. Bravo-Suárez, R.V. Chaudhari, B. Subramaniam, Design of Heterogeneous Catalysts for Fuels and Chemicals Processing: An Overview in: *Novel Materials for Catalysis and Fuels Processing*, J.J. Bravo-Suárez, M.K. Kidder, V. Schwartz, Eds., American Chemical Society, Washington, D.C., 2013, pp. 3-68.
19 C. Lamberti, A. Zecchina, E. Groppo, S. Bordiga, *Chem. Soc. Rev.*, 2010, **39**, 4951-5001.
20 C. Hess, *Top. Catal.*, 2013, **56**, 1593-1600.
21 J.J. Bravo-Suárez, P.D. Srinivasan, *Catal. Rev.- Sci. Eng.*, 2017, pp1-151, https://doi.org/110.1080/01614940.01612017.01360071.
22 H. Topsøe, *J. Catal.*, 2003, **216**, 155-164.
23 F.C. Meunier, *React. Chem. Eng.*, 2016, **1**, 134-141.
24 M.A. Bañares, *Catal. Today*, 2005, **100**, 71-77.
25 F.C. Jentoft, *Adv. Catal.*, 2009, **52**, 129-211.
26 S.T. Oyama, W. Zhang, *J. Am. Chem. Soc.*, 1996, **118**, 7173-7177.
27 K. Tamaru, Dynamic heterogeneous catalysis, Academic Press, New York, NY, 1978, pp. 1-140.
28 A. Ueno, T. Onishi, K. Tamaru, *Trans. Faraday Soc.*, 1970, **66**, 756-763.
29 K. Tamaru, *Adv. Catal.*, 1965, **15**, 65-90.
30 R. Kopelent, J.A. van Bokhoven, J. Szlachetko, J. Edebeli, C. Paun, M. Nachtegaal, O.V. Safonova, *Angew. Chem., Int. Ed.*, 2015, **54**, 8728-8731.
31 N. Maeda, F. Meemken, K. Hungerbühler, A. Baiker, *Chimia*, 2012, **66**, 664-667.
32 S.C. Reyes, E. Iglesia, Frequency response techniques for the characterization of porous catalytic solids in: *Catalysis*, J.J. Spivey, S.K. Agarwal, Eds., The Royal Society of Chemistry, 1994, pp. 51-92.
33 P.L. Silverton (Ed.), In: *Composition Modulation of Catalytic Reactors (Topics in Chemical Engineering, Vol. 11)*, Gordon and Breach Science Publishers, Amsterdam (The Netherlands), 1998, pp. 1-596
34 V. Marchionni, D. Ferri, O. Krocher, A. Wokaun, *Anal. Chem.*, 2017, **89**, 5802-5810.
35 Y. Yang, R.S. Disselkamp, J. Szanyi, C.H.F. Peden, C.T. Campbell, J.G. Goodwin, *Rev. Sci. Instrum.*, 2006, **77**, 094104.
36 G. Mirth, F. Eder, J.A. Lercher, *Appl. Spectrosc.*, 1994, **48**, 194-197.
37 J. Wang, V.F. Kispersky, W.N. Delgass, F.H. Ribeiro, *J. Catal.*, 2012, **289**, 171-178.
38 P.D. Srinivasan, S.R. Nitz, K.J. Stephens, E. Atchison, J.J. Bravo-Suarez, *Appl. Catal., A*, 2018, **561**, 7-18.
39 J.J. Venter, M.A. Vannice, *Appl. Spectrosc.*, 1988, **42**, 1096-1103.
40 J. Kritzenberger, A. Wokaun, *J. Mol. Catal. A: Chem.*, 1997, **118**, 235-245.
41 E.E. Ortelli, A. Wokaun, *Vib. Spectrosc.*, 1999, **19**, 451-459.
42 E.E. Ortelli, J. Wambach, A. Wokaun, *Appl. Catal., A*, 2000, **192**, 137-152.
43 E.E. Ortelli, J. Wambach, A. Wokaun, *Appl. Catal., A*, 2001, **216**, 227-241.
44 M. Cavers, J.M. Davidson, I.R. Harkness, G.S. McDougall, L.V.C. Rees, *Stud. Surf. Sci. Catal.*, 1999, **122**, 65-72.

45 M. Cavers, J.M. Davidson, I.R. Harkness, L.V.C. Rees, G.S. McDougall, *J. Catal.*, 1999, **188**, 426-430.
46 R. Kydd, D. Ferri, P. Hug, J. Scott, W.Y. Teoh, R. Amal, *J. Catal.*, 2011, **277**, 64-71.
47 A. Haghofer, D. Ferri, K. Fottinger, G. Rupprechter, *ACS Catal.*, 2012, **2**, 2305-2315.
48 O. Martin, C. Mondelli, A. Cervellino, D. Ferri, D. Curulla-Ferre, J. Perez-Ramirez, *Angew. Chem., Int. Ed.*, 2016, **55**, 11031-11036.
49 G.L. Chiarello, M. Nachtegaal, V. Marchionni, L. Quaroni, D. Ferri, *Rev. Sci. Instrum.*, 2014, **85**, 074102.
50 J. Zarfl, D. Ferri, T.J. Schildhauer, J. Wambach, A. Wokaun, *Appl. Catal., A*, 2015, **495**, 104-114.
51 V. Marchionni, M.A. Newton, A. Kambolis, S.K. Matam, A. Weidenkaff, D. Ferri, *Catal. Today*, 2014, **229**, 80-87.
52 M. Nobutaka, M. Fabian, B. Alfons, *ChemCatChem*, 2013, **5**, 2199-2202.
53 A. Aguirre, S.E. Collins, *Catal. Today*, 2013, **205**, 34-40.
54 J. Vecchietti, A. Bonivardi, W.Q. Xu, D. Stacchiola, J.J. Delgado, M. Calatayud, S.E. Collins, *ACS Catal.*, 2014, **4**, 2088-2096.
55 E. del Rio, S.E. Collins, A. Aguirre, X.W. Chen, J.J. Delgado, J.J. Calvino, S. Bernal, *J. Catal.*, 2014, **316**, 210-218.
56 A. Aguirre, C.E. Barrios, A. Aguilar-Tapia, R. Zanella, M.A. Baltanas, S.E. Collins, *Top. Catal.*, 2016, **59**, 347-356.
57 P. Müller, S.P. Burt, A.M. Love, W.P. McDermott, P. Wolf, I. Hermans, *ACS Catal.*, 2016, **6**, 6823-6832.
58 M.A. Newton, *Top. Catal.*, 2009, **52**, 1410-1424.
59 B. Li, R.D. Gonzalez, *Appl. Spectrosc.*, 1998, **52**, 1488-1491.
60 M.M. Schubert, T.P. Häring, G. Bräth, H.A. Gasteiger, R.J. Behm, *Appl. Spectrosc.*, 2001, **55**, 1537-1543.
61 V. Dal Santo, C. Dossi, A. Fusi, R. Psaro, C. Mondelli, S. Recchia, *Talanta*, 2005, **66**, 674-682.
62 H.S. Fogler, Chapter 13: Distribution of Residence Times for Chemical Reactors in: *Elements of Chemical Reaction Engineering*, 4th ed., Prentice Hall, Upper Saddle River, NJ, 2005, pp. 867-944.
63 O. Levenspiel, Chemical Reaction Engineering, 3rd ed., Wiley, New York, NY, 1999, pp. 1-668.
64 R.B. Bird, W.E. Stewart, E.N. Lightfoot, Transport Phenomena, 2nd Ed., Wiley, New York, 2002, pp. 1-895.
65 D.E. Newland, An Introduction to Random Vibrations and Spectral Analysis, Longman, Mineola, NY, 1984, pp. 1-477.
66 M. Karam, H.F. Khazaal, H. Aglan, C. Cole, *J. Signal Inf. Proc.*, 2014, **5**, 32-41.
67 M.L. Meade, Lock-in Amplifiers: Principles and Applications, P. Peregrinus, London, UK, 1983, pp. 1-232.
68 J.A. Dávila Pintle, *Rev. Mex. Fis. E*, 2013, **59**, 1-7.
69 J.A.T.A. Dantas, P.R. Pegoraro, J.A.W. Gut, *Int. J. Heat Mass Transfer*, 2014, **71**, 18-25.
70 H. Li, M. Rivallan, F. Thibault-Starzyk, A. Travert, F.C. Meunier, *Phys. Chem. Chem. Phys.*, 2013, **15**, 7321-7327.
71 J. Lee, J. Szanyi, J.H. Kwak, *Mol. Catal.*, 2017, **434**, 39-48.
72 J. Lee, E.J. Jang, H.Y. Jeong, J.H. Kwak, *Appl. Catal., A*, 2018, **556**, 121-128.
73 K.K. Priya D. Srinivasan, John Meynard M. Tengco, Hongda Zhu, Juan J. Bravo-Suárez, 2018, Submitted.
74 T.K. Phung, A. Lagazzo, M.A.R. Crespo, V.S. Escribano, G. Busca, *J. Catal.*, 2014, **311**, 102-113.
75 T.K. Phung, G. Busca, *Chem. Eng. J. (Lausanne)*, 2015, **272**, 92-101.
76 M.A. Natal-Santiago, J.A. Dumesic, *J. Catal.*, 1998, **175**, 252-268.
77 P.Y. Sheng, G.A. Bowmaker, H. Idriss, *Appl. Catal., A*, 2004, **261**, 171-181.
78 H.A. Al-Abadleh, V.H. Grassian, *Langmuir*, 2003, **19**, 341-347.
79 K. Alexopoulos, M.-S. Lee, Y. Liu, Y. Zhi, Y. Liu, M.-F. Reyniers, G.B. Marin, V.-A. Glezakou, R. Rousseau, J.A. Lercher, *J. Phys. Chem. C*, 2016, **120**, 7172-7182.
80 M. Nedic, T.N. Wassermann, R.W. Larsen, M.A. Suhm, *Phys. Chem. Chem. Phys.*, 2011, **13**, 14050-14063.
81 K. Hadjiivanov, Identification and Characterization of Surface Hydroxyl Groups by Infrared Spectroscopy in: *Advances in Catalysis, Vol 57*, F.C. Jentoft, Ed., 2014, pp. 99-318.
82 G. Busca, Structural, Surface, and Catalytic Properties of Aluminas in: *Advances in Catalysis, Vol 57*, F.C. Jentoft, Ed., 2014, pp. 319-404.
83 M. Digne, P. Sautet, P. Raybaud, P. Euzen, H. Toulhoat, *J. Catal.*, 2002, **211**, 1-5.
84 J.F. DeWilde, H. Chiang, D.A. Hickman, C.R. Ho, A. Bhan, *ACS Catal.*, 2013, **3**, 798-807.
85 J.I. Di Cosimo, V.K. Díez, M. Xu, E. Iglesia, C.R. Apesteguía, *J. Catal.*, 1998, **178**, 499-510.
86 J.H. Kwak, D. Mei, C.H.F. Peden, R. Rousseau, J. Szanyi, *Catal. Lett.*, 2011, **141**, 649-655.

Design, Modelling, and Application of a Low Void-Volume in Situ Diffuse Reflectance Spectroscopic Reaction Cell for Transient Catalytic Studies

Bhagyesha S. Patil, Priya D. Srinivasan, Ed Atchison, Hongda Zhu, Juan J. Bravo-Suárez

A new low void-volume in situ reaction cell enables application of modulation excitation-phase sensitive detection-diffuse reflectance Fourier transform spectroscopy (ME-PSD-DRIFTS)